Supporting Information

MOF-derived N-doped C @ CoO/MoC Heterojunction Compo-site for Efficient Oxygen Reduction Reaction and Long-life Zn-air Battery

Ruilian Yin,[1, 3] Suli Ma,[1] Jiaping Ying,[1] Zhentao Lu,[4] Xinxin Niu,[2] Jinxiu Feng,[2] Feng Xu,[1] Yifan Zheng,[1] Wenxian Liu[2*] and Xiehong Cao[2,3*]

[1] College of Chemical Engineering, Zhejiang University of Technology, Hangzhou 310014, China

[2] College of Materials Science and Engineering, Zhejiang University of Technology, 18 Chaowang Road, Hangzhou 310014, China

[3] Pinghu Institute of Advanced Materials, Zhejiang University of Technology, Jiaxing 314213, China

[4] College of Information Engineering, Zhejiang University of Technology, Hangzhou 310014, China

*Corresponding author. E-mail: gcscaoxh@zjut.edu.cn and liuwx@zjut.edu.cn.

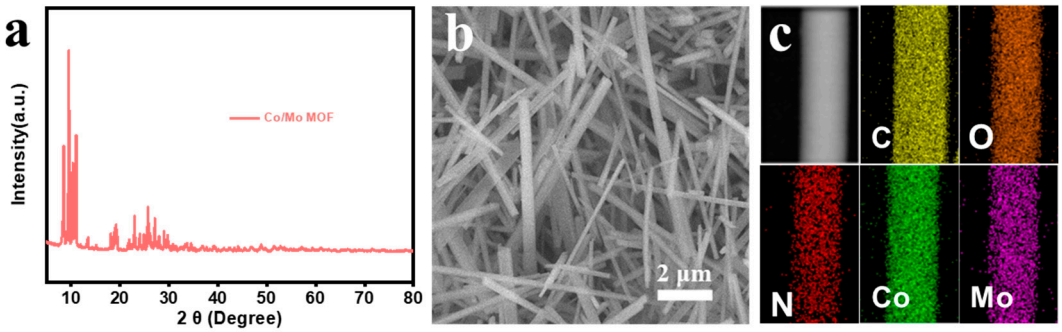

Figure S1 (a) XRD patterns (b) SEM images and (c) EDX elemental mapping images of Co/Mo MOF.

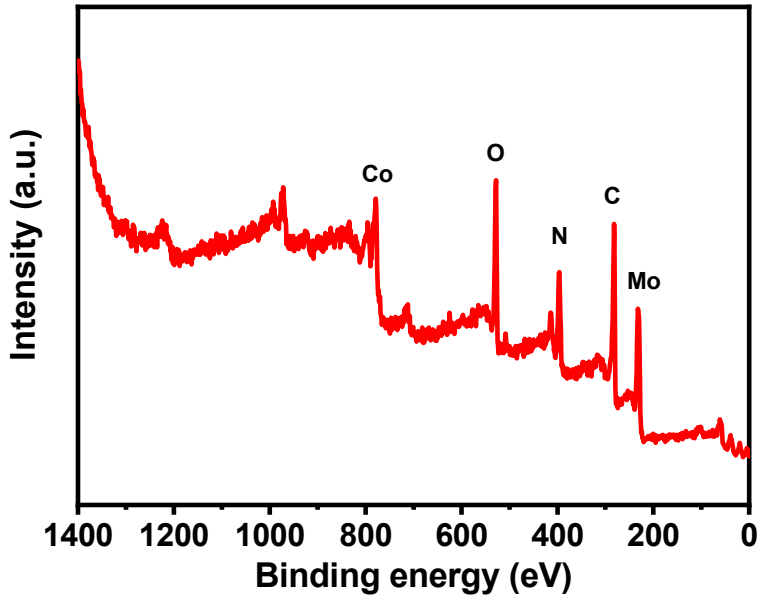

Figure S2 Full-survey XPS spectra of the CoO/MoC@N/C heterojunction composite.

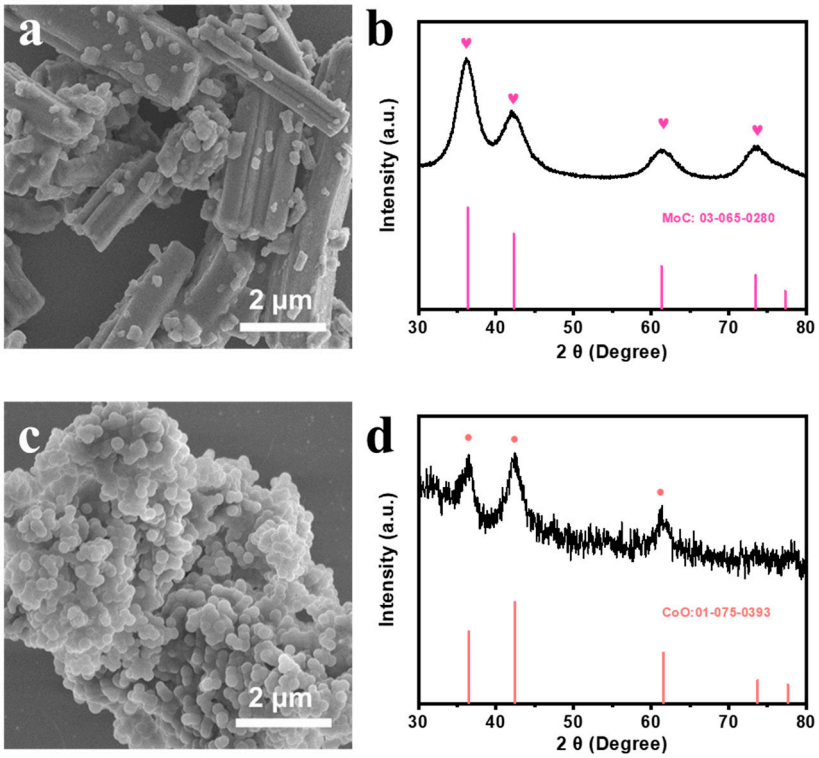

Figure S3 SEM images and XRD patterns of (a-b) Mo MOF derived MoC and (c-d) Co MOF derived CoO.

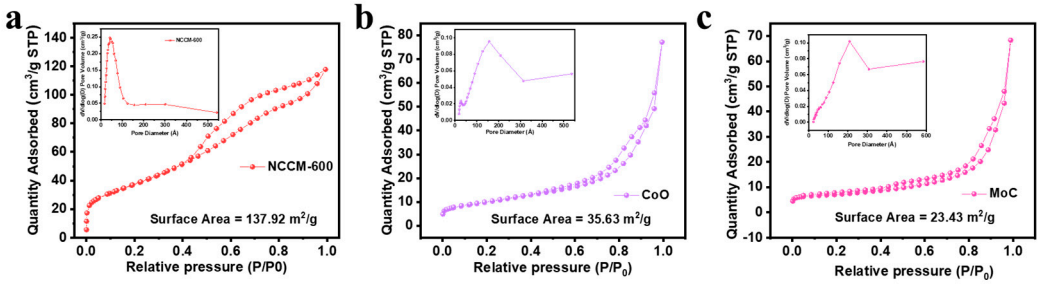

Figure S4 Nitrogen adsorption-desorption isotherms and corresponding pore-size distribution of (a) NCCM-600 (b) Co MOF derived CoO and (c) Mo MOF derived MoC.

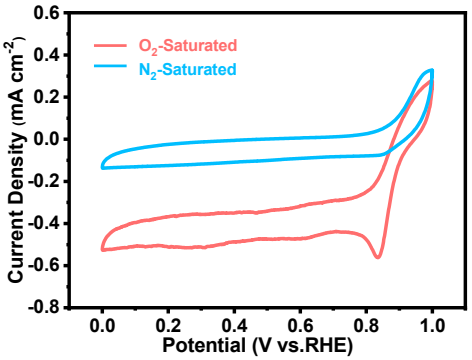

Figure S5 (a) CV curves of NCCM-600 heterojunction composite in 0.1 m KOH saturated with O_2 and N_2.

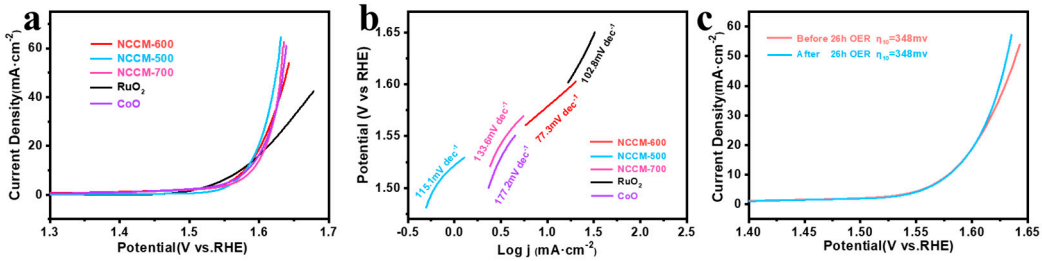

Figure S6 (a) Linear sweep voltammetry (LSV) curves and (b) corresponding Tafel plots of NCCM-500, NCCM -600, NCCM -700, commercial RuO_2 and CoO (c) The stability of polarization curves of the NCCM-600.

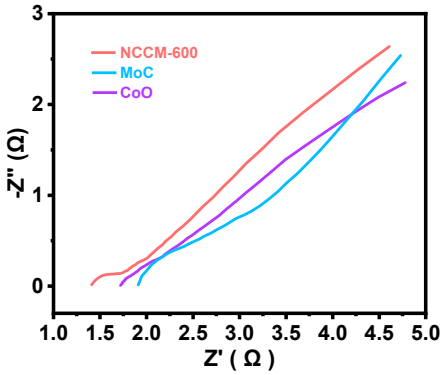

Figure S7 Nyquist plots of MOF derived N-doped porous C@CoO/MoC heterojunction composite, MOF derived MoC and MOF derived CoO.

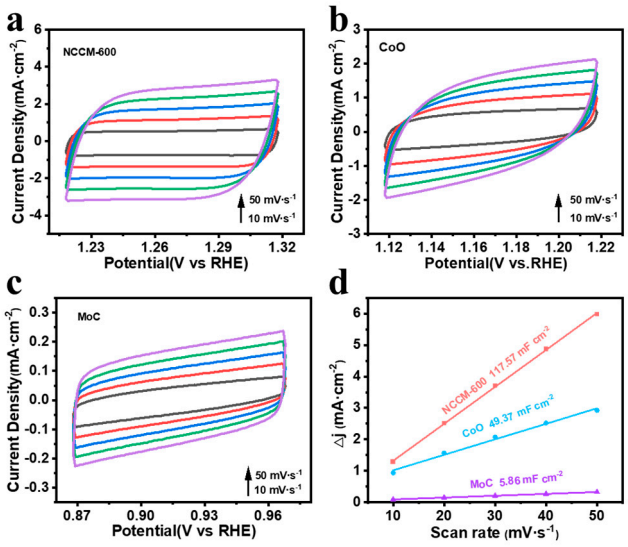

Figure S8 CV curves of prepared (a) NCCM-600 (b) CoO (c) MoC in 1 M KOH at different scan rates. (d) Calculated C_{dl} for different samples, charging current density differences plotted against scan rate of the electrodes. The linear slope was used to represent the ECSA.

Catalysts	$E_{1/2(ORR)}$ (V)	$E_{j=10(OER)}$ (V)	$\Delta E=E_{j=10}-E_{1/2}$ (V)	References
NCCM-600	**0.843**	**1.577**	**0.734**	**This work**
Co_3O_4@CoO@Co	0.79	1.65	0.86	[1]
In-CoO/CoP FNS	0.81	1.597	0.787	[2]
NSC-CoO-900	0.83	1.66	0.83	[3]
CoO/hi-Mn_3O_4	0.70	1.60	0.90	[4]
CoO@NSNGs	0.82	1.63	0.81	[5]
MoC	0.72	-		[6]
CNF@Zn/CoNC	0.82	1.70	0.88	[7]
Ni-Fe-MoN NTs	0.72	1.53	0.81	[8]
Mo-N/C@MoS_2	0.81	1.62	0.81	[9]
2H-MoS_2	0.66	1.73	1.07	[10]
Co@IC/MoC@PC	0.875	1.512	0.635	[11]
P–CoO@PWC–2	0.84	1.52	0.68	[12]

Table S1 Comparison of the overpotentials for ORR (at $E_{1/2}$) and OER at (10 mA cm^{-2}) of the prepared CoO/MoC@N/C heterojunction composite and other reported bifunctional electrocatalysts.

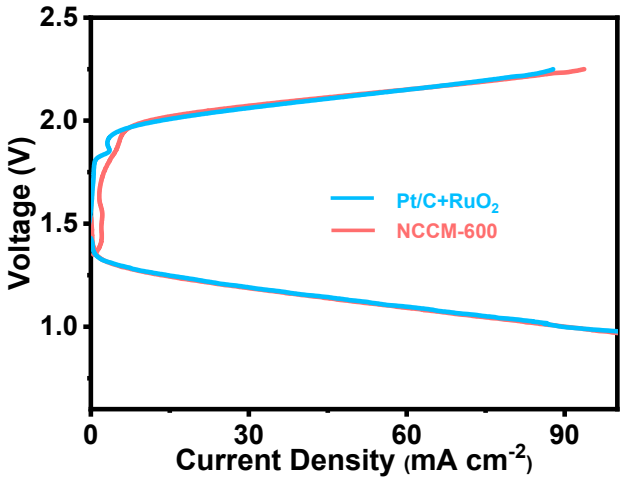

Figure S9 Charge and discharge polarization curves of the fabricated Zn-air batteries.

References

1. Chou, S. C., Tso, K. C., et al. Facile synthesis of Co_3O_4@ CoO@ Co gradient core@ shell nanoparticles and their applications for oxygen evolution and reduction in alkaline electrolytes. *Materials*, **2020**, 13(12): 2703.
2. Jin W, Chen J, Liu B, et al. Oxygen Vacancy–Rich In–Doped CoO/CoP Heterostructure as an Effective Air Cathode for Rechargeable Zn–Air Batteries[J]. *Small*, **2019**, 15(46): 1904210.
3. Chen S, Chen S, Zhang B, et al. Bifunctional oxygen electrocatalysis of N, S-codoped porous carbon with interspersed hollow CoO nanoparticles for rechargeable Zn–air batteries[J]. *ACS applied materials & interfaces*, **2019**, 11(18): 16720-16728.
4. Guo C, Zheng Y, Ran J, et al. Engineering high–energy interfacial structures for high - performance oxygen–involving electrocatalysis[J]. *Angewandte Chemie International Edition*, **2017**, 56(29): 8539-8543.
5. Zhang M, Han C, Cao W Q, et al. A nano-micro engineering nanofiber for electromagnetic absorber, green shielding and sensor[J]. *Nano-micro letters*, **2021**, 13(1): 1-12.
6. Defo C, Mishra A K, Yerima B P K, et al. Current conditions of groundwater resources development and related problems in the Republic of Cameroon, West Africa[J]. *European Water*, **2016**, 54: 43-68.
7. Zhao Y, Lai Q, Zhu J, et al. Controllable construction of core–shell polymer@ zeolitic imidazolate frameworks fiber derived heteroatom - doped carbon nanofiber network for efficient oxygen electrocatalysis[J]. *Small*, **2018**, 14(19): 1704207.
8. Tomon C, Sarawutanukul S, Duangdangchote S, et al. Photoactive Zn–air batteries using spinel-type cobalt oxide as a bifunctional photocatalyst at the air cathode[J]. *Chemical Communications*,

2019, 55(42): 5855-5858.

9. Sadighi Z, Liu J, Zhao L, et al. Metallic MoS 2 nanosheets: multifunctional electrocatalyst for the ORR, OER and Li–O 2 batteries[J]. *Nanoscale*, **2018**, 10(47): 22549-22559.
10. Ouyang B, Artrith N, Lun Z, et al. Effect of Fluorination on Lithium Transport and Short‐Range Order in Disordered‐Rocksalt‐Type Lithium‐Ion Battery Cathodes[J]. *Advanced Energy Materials*, **2020**, 10(10): 1903240.
11. Zhang L, Zhu Y, Nie Z, et al. Co/MoC nanoparticles embedded in carbon nanoboxes as robust trifunctional electrocatalysts for a Zn–air battery and water electrocatalysis[J]. *ACS nano*, **2021**, 15(8): 13399-13414.
12. Liu H, Liu Y, Mehdi S, et al. Surface Phosphorus‐Induced CoO Coupling to Monolithic Carbon for Efficient Air Electrode of Quasi‐Solid‐State Zn-Air Batteries[J]. *Advanced Science*, **2021**, 8(19), 2101314.